

On the Galactic chemical evolution of sulphur

Sulphur abundances from the [S I] λ 1082 nm line in giants ^{*,**}

E. Matrozis¹, N. Ryde¹, and A. K. Dupree²

¹ Department of Astronomy and Theoretical Physics, Lund Observatory, Lund University, Box 43, 221 00, Lund, Sweden
e-mail: ryde@astro.lu.se

² Harvard-Smithsonian Center for Astrophysics, 60 Garden St., Cambridge, MA 02138, USA

Received ; accepted

ABSTRACT

Context. The Galactic chemical evolution of sulphur is still under debate. At low metallicities some studies find no correlation between [S/Fe] and [Fe/H], which is typical for other α -elements, while others find [S/Fe] increasing towards lower metallicities, and still others find a combination of the two. Each scenario has different implications for the Galactic chemical evolution of sulphur.

Aims. The aim of this study is to contribute to the discussion on the Galactic chemical evolution of sulphur by deriving sulphur abundances from non-LTE insensitive spectral diagnostics in Disk and Halo stars with homogeneously determined stellar parameters.

Methods. We derive effective temperatures from photometric colours, surface gravities from stellar isochrones and Bayesian estimation, and metallicities and sulphur abundances from spectrum synthesis. We derive sulphur abundances from the [S I] λ 1082 nm line in 39 mostly cool and metal-poor giants, using 1D LTE MARCS model atmospheres to model our high-resolution near-infrared spectra obtained with the VLT, NOT and Gemini South telescopes.

Results. We derive homogeneous stellar parameters for 29 of the 39 stars. Our results argue for a chemical evolution of sulphur that is typical for α -elements, contrary to some previous studies that have found high sulphur abundances ([S/Fe] \geq 0.6) for stars with $-2.5 < [\text{Fe}/\text{H}] < -1$. Our abundances are systematically higher by about 0.1 dex in comparison to other studies that arrived at similar conclusions using other sulphur diagnostics.

Conclusions. We find the [S I] line to be a valuable diagnostic of sulphur abundances in cool giants down to [Fe/H] ≈ -2.3 . We argue that a homogeneous determination of stellar parameters is necessary, since the derived abundances are sensitive to them. Our results ([S/Fe]) show reasonable agreement with predictions of contemporary models of Galactic chemical evolution. In these models sulphur is predominantly created in massive stars by oxygen burning, and ejected in the interstellar medium during Type II supernovae explosions. Systematic differences with previous studies likely fall within modelling uncertainties.

Key words. Galaxy: evolution – stars: fundamental parameters – stars: abundances – infrared: stars

1. Introduction

Sulphur is a chemical element of considerable scientific interest. First, it is one of the α -elements, which are elements from O to Ti with even atomic numbers. Studies of α -element abundances in stellar atmospheres can shed light on such important properties of stellar populations as their star-formation history and initial mass function (e.g., McWilliam 1997). These properties are needed for the discussion on how galaxies are formed and how they evolve.

Second, sulphur is a volatile element. As such, it does not form dust easily and the number of its atoms measured in a gas is indeed the total number, which makes sulphur suitable for cosmological studies. In particular, it (together with another volatile, zinc) could be used as a cosmological clock in tracing the evolution of damped Ly α systems (Nissen et al. 2004; Nissen et al.

2007) – huge clouds of predominantly neutral hydrogen gas at high redshifts that are thought to play an instrumental role in the formation of galaxies. Before this discussion can be had, however, the chemical evolution of sulphur has to be understood in our own Galaxy.

Observational studies of Galactic chemical evolution of sulphur were scarce before early 2000s due to the lack of suitable spectral diagnostics, and concerned mainly stars with [Fe/H] > -1 (e.g., Wallerstein & Conti 1964; Francois 1987, 1988). This has changed partly due to the advent of infrared detector arrays. Now several studies on sulphur abundances in metal-poor stars have been published and left the matter of whether sulphur is a typical α -element controversial. To summarize (see Jönsson et al. (2011) for a more in-depth review of the methods and findings of previous studies), early studies by Israelian & Rebolo (2001) and Takada-Hidai et al. (2002) found that the relative sulphur abundance continuously increases in the metallicity range from solar down to at least [Fe/H] ≈ -2.5 , implying a different chemical evolution history from that of other α -elements which display a (nearly) metallicity-independent enrichment with respect to iron in stars of low ([Fe/H] $\lesssim -1$)

* Based partly on observations obtained at the Gemini Observatory, which is operated by the AURA, Inc., under a cooperative agreement with the NSF on behalf of the Gemini partnership: the NSF (US), the PPARC (UK), the NRC (Canada), CONICYT (Chile), the ARC, CNPq (Brazil), and CONICET (Argentina).

** Based partly on observations collected at the European Southern Observatory, Chile (ESO program 080.D-0675).

metallicity (Cayrel et al. 2004; Jonsell et al. 2005).¹ A high rate of sulphur-rich hypernovae (e.g., Nakamura et al. 2001) and a time-delayed deposition of iron into the interstellar medium (Ramaty et al. 2000) have been proposed as possible explanations for these unexpected results. On the other hand, a number of studies (e.g., Ryde & Lambert 2004; Korn & Ryde 2005; Nissen et al. 2007; Spite et al. 2011) have found little to no evidence of high ($[S/Fe] \gtrsim 0.6$) sulphur abundances at any metallicity, instead arguing for sulphur being a fairly typical α -element and forming a plateau of $[S/Fe] \sim 0.3$ below $[Fe/H] \sim -1$, which points to an origin in Type II supernovae (e.g., Kobayashi et al. 2006). Finally, a combination of the two patterns, which implies a very complex history of chemical evolution of sulphur, has been found by Caffau et al. (2005) and Caffau et al. (2010).

The question of whether there exist metal-poor stars with extremely high sulphur abundances is open to debate, and the discrepant findings of previous studies could either reflect reality or differences in the employed analyses. Among these are the differences in sulphur diagnostics employed, stellar parameters adopted and the types of stars analysed, and assumptions made regarding the dimensionality and local thermodynamic equilibrium (LTE; for a discussion on the effects of these assumptions see, e.g., Takada-Hidai et al. 2005; Takeda et al. 2005; Jönsson et al. 2011). In this 1D LTE study of sulphur abundances in cool giants we aim to mitigate some of these concerns:

1. instead of adopting the stellar parameters (T_{eff} , $\log g$ and $[Fe/H]$) from multiple previous studies, as most of the studies concerning sulphur have done, we determine them using a single methodology to avoid introducing additional scatter in the results;
2. only the $[S\text{I}] \lambda 1082$ nm line is used to derive sulphur abundances. This forbidden line is insensitive to the assumption of LTE putting at least one of the two main modelling assumptions – radial symmetry and local thermodynamic equilibrium – on a more solid footing.

2. Observations

While we are mainly interested in sulphur abundances in stars with $[Fe/H] < -1$, about half of our sample consists of more metal-rich stars. The sample is combined from four subsamples: 1) 14 “disk” ($[Fe/H] > -1$) stars from Ryde (2006) observed with the Gemini South telescope (Phoenix spectrometer) with $R = \lambda/\Delta\lambda \simeq 60\,000$ and $S/N \simeq 200$; 2) the metal-poor ($[Fe/H] < -1$) sample observed by Ryde within the same programme, but previously unpublished; 3) data from Jönsson et al. (2011) obtained at VLT (CRIRES) with $R \simeq 80\,000$ and S/N between about 250 and 500 for most stars (HD 13979 and HD 103545 have S/N of 570 and 160, respectively); 4) three metal-deficient ($[Fe/H] \sim -0.4$) stars observed by Ilyin (2000) with the NOT (SOFIN) with $R \simeq 80\,000$ and $S/N \simeq 70$. The wavelength coverage is about 5 nm ($\lambda \simeq 1080\text{--}1085$ nm) for the Phoenix and SOFIN data and about 10 nm ($\lambda \simeq 1080\text{--}1092$ nm) with a 2 nm gap around 1086 nm) for the CRIRES data. We refer to the publications of Ryde (2006), Jönsson et al. (2011) and Ilyin (2000) for detailed descriptions of subsamples 1-2, 3 and 4, respectively. Basic data of the sample stars is given in Table 1.

¹ The abundance of an element A with respect to element B is $[A/B] = \log_{10}(N_A/N_B)_* - \log_{10}(N_A/N_B)_\odot$ where N is the number density. We call $[Fe/H]$ the metallicity and $[S/Fe]$ the sulphur abundance.

3. Analysis

In this section we describe the determination of stellar parameters (Sect. 3.1) and sulphur abundances (Sect. 3.2).

3.1. Stellar parameters

3.1.1. Effective temperature

The effective temperatures were derived from the photometric colour-effective temperature calibrations of González Hernández & Bonifacio (2009). In particular, we used photometric data from the Johnson and 2MASS photometric systems to derive T_{eff} from the $B - V$, $V - J$, $V - H$, $V - K_s$ and $J - K_s$ colours.

Each colour gives an estimate of effective temperature $T_{\text{eff},i} = 5040 \text{ K}/\theta_{\text{eff},i}$, where

$$\theta_{\text{eff},i} = a_0 + a_1 X_i + a_2 X_i^2 + a_3 X_i [Fe/H] + a_4 [Fe/H] + a_5 [Fe/H]^2, \quad (1)$$

X_i is the (de-reddened) colour, and a_j are the coefficients of the respective calibration. We then adopted a weighted mean effective temperature according to

$$\bar{T}_{\text{eff}} = \frac{\sum w_i T_{\text{eff},i}}{\sum w_i}, \quad (2)$$

where $w_i = (\Delta T_{\text{eff},i})^{-2}$. The uncertainties in the individual estimates ($\Delta T_{\text{eff},i}$) are formally propagated uncertainties in the colours, metallicities, colour excesses, and the calibrations themselves. We adopted the weighted mean of the squared deviations from \bar{T}_{eff} as the uncertainty of the temperatures:

$$\Delta \bar{T}_{\text{eff}} = \frac{\sum w_i (T_{\text{eff},i} - \bar{T}_{\text{eff}})^2}{\sum w_i}. \quad (3)$$

The Johnson V magnitudes and $B - V$ colours and their uncertainties were taken from the General Catalogue of Photometric Data (GCPD; Mermilliod et al. 1997). The mean uncertainty in V and $B - V$ for the sample is ~ 0.014 and ~ 0.008 mag, respectively, which motivated our assumption of $\Delta V = 0.015$ and $\Delta(B - V) = 0.010$ mag for stars that had no error estimates in the catalogue. A few stars (see Table 1) had no entries in GCPD, and their V magnitudes and $B - V$ colours were taken from Rossi et al. (2005).

The 2MASS magnitudes and their uncertainties were taken from the 2MASS All-Sky Point Source Catalog (Skrutskie et al. 2006). The 2MASS magnitudes generally have good precision (quality flag A) for $JHK_s \gtrsim 5$, which is the case for about a half of our sample. For the other half the uncertainties are considerably larger, introducing an uncertainty of a few hundred K in each $T_{\text{eff},i}$. For these stars we chose to invert the colour transformations of Ramírez & Meléndez (2005a) to derive the 2MASS JHK_s magnitudes from the JHK magnitudes of the TCS photometric system (Alonso et al. 1994; Alonso et al. 1998). The agreement between measured and calculated 2MASS magnitudes for faint stars was found to be excellent. While there is no good reason to assume that the transformation is valid for bright stars, we find good agreement between measured 2MASS (that have large uncertainties) and calculated-from-TCS 2MASS (small uncertainties) magnitudes for them, which indicates that the extrapolation is at the very least valid within the uncertainties of the observed magnitudes. Hence, in order of preference we adopted: 1) measured 2MASS magnitudes (when the quality flag was A); 2) TCS magnitudes transformed to the 2MASS system (when the quality flag was C or worse); 3) 2MASS magnitudes with quality flags of C or worse when no TCS data were available.

Table 1. Basic data of the analysed stars.

Star identifier		RA(J2000) ^a	Dec(J2000) ^a	π^a	V^b	$B - V^b$	Ref. ^b	E_{B-V}^c	JHK_s	Subsample ^e
HD/BD	HIP	(h m s)	(d m s)	(mas)					flag ^d	
2796	2463	00 31 16.915	-16 47 40.79	0.88 ± 0.81	8.495	0.747	1	0.020	AAA	2
3546	3031	00 38 33.345	+29 18 42.28	19.91 ± 0.19	4.361	0.871	1	0.008	TCS	1
8724	6710	01 26 17.594	+17 07 35.11	2.52 ± 0.71	8.300	0.987	1	0.106	AAA	2
10380	7884	01 41 25.894	+05 29 15.39	8.98 ± 0.23	4.437	1.364	1	0.016	TCS	1
13979	10497	02 15 20.853	-25 54 54.86	0.46 ± 1.13	0.012	AAA	3
21581	16214	03 28 54.486	-00 25 03.09	4.03 ± 1.00	8.710	0.825	1	0.069	AAA	3
23798	17639	03 46 45.722	-30 51 13.35	1.83 ± 0.74	8.302	1.098	1	0.008	AAA	3
26297	19378	04 09 03.418	-15 53 27.07	1.59 ± 0.78	7.470	1.110	1	0.030	AEA	3
29574	21648	04 38 55.733	-13 20 48.13	1.40 ± 0.88	8.336	1.401	1	0.183	AEA	3
34334	24727	05 18 10.569	+33 22 17.86	14.04 ± 0.58	4.538	1.266	1	0.014	TCS	4
36702	25916	05 31 52.230	-38 33 24.04	0.46 ± 0.58	8.365	1.216	1	0.028	AAA	3
37160	26366	05 36 54.389	+09 17 26.41	27.76 ± 0.27	4.082	0.958	1	0.008	TCS	4
40460	28417	06 00 06.039	+27 16 19.87	6.90 ± 0.56	6.609	1.022	1	0.026	CCD	1
44007	29992	06 18 48.528	-14 50 43.44	5.57 ± 0.84	8.059	0.839	1	0.033	AAA	3
65953	39211	08 01 13.336	-01 23 33.37	7.25 ± 0.30	4.676	1.491	1	0.009	DDD	4
81192	46155	09 24 45.336	+19 47 11.88	8.62 ± 0.46	6.530	0.947	1	0.016	TCS	1
83212	47139	09 36 19.952	-20 53 14.74	0.96 ± 0.77	8.335	1.070	1	0.059	AAA	3
85773	48516	09 53 39.242	-22 50 08.41	3.41 ± 1.20	9.380	1.120	1	0.027	AAA	3
103545	58139	11 55 27.163	+09 07 45.00	0.12 ± 1.35	9.200	0.710	2	0.034	AAA	3
110184	61824	12 40 14.079	+08 31 38.07	0.76 ± 0.84	8.305	1.175	1	0.020	AAA	2
111721	62747	12 51 25.196	-13 29 28.22	4.33 ± 0.86	7.971	0.799	1	0.038	AAA	2
117876	66086	13 32 48.214	+24 20 48.31	7.43 ± 0.57	6.092	0.965	1	0.008	TCS	1
122563	68594	14 02 31.846	+09 41 09.95	4.22 ± 0.35	6.200	0.904	1	0.019	TCS	2
122956	68807	14 05 13.026	-14 51 25.46	3.16 ± 0.59	7.220	1.010	1	0.065	AEA	2
139195	76425	15 36 29.579	+10 00 36.62	14.11 ± 0.30	5.260	0.945	1	0.011	TCS	1
161074	86667	17 42 28.362	+24 33 50.58	8.04 ± 0.36	5.525	1.452	1	0.028	DCD	1
166161	88977	18 09 40.687	-08 46 45.60	4.56 ± 0.84	8.120	0.976	1	0.293	AAA	2
168723	89962	18 21 18.601	-02 53 55.68	53.93 ± 0.18	3.254	0.941	1	0.016	TCS	1
184406	96229	19 34 05.353	+07 22 44.21	30.31 ± 0.24	4.450	1.177	1	0.005	TCS	1
187111	97468	19 48 39.575	-12 07 19.74	1.45 ± 0.82	7.720	1.225	1	0.124	AEA	2
188512	98036	19 55 18.792	+06 24 24.45	73.00 ± 0.20	3.715	0.855	1	0.003	DCD	1
204543	106095	21 29 28.213	-03 30 55.38	-0.13 ± 1.08	8.600	0.760	2	0.034	AAA	2
212943	110882	22 27 51.522	+04 41 44.41	21.99 ± 0.37	4.794	1.051	1	0.021	TCS	1
214567	111810	22 38 52.589	+19 31 20.16	8.74 ± 0.44	5.820	0.925	1	0.013	DCD	1
216143	112796	22 50 31.089	-06 54 49.54	0.87 ± 0.91	8.200	0.940	2	0.039	AAA	2
219615	114971	23 17 09.938	+03 16 56.23	23.64 ± 0.18	3.696	0.921	1	0.015	DDD	1
220954	115830	23 27 58.096	+06 22 44.37	21.96 ± 0.25	4.279	1.076	1	0.014	TCS	1
221170	115949	23 29 28.809	+30 25 57.86	2.94 ± 0.69	7.674	1.085	1	0.086	AAA	2
+30 2611	73960	15 06 53.830	+30 00 36.95	1.07 ± 1.23	9.123	1.240	1	0.021	AAA	2

Notes. ^a taken from van Leeuwen (2007); ^b taken from: 1 – Mermilliod et al. (1997), 2 – Rossi et al. (2005); ^c derived in this work (see Sect. 3.1.1); ^d 2MASS photometry quality flags for colours J , H and K_s (Skrutskie et al. 2006). TCS – colours transformed to 2MASS system from the TCS system (see text). The H magnitude of HD 26297, 29574 and 187111 was also transformed from the TCS system; ^e as defined in Sect. 2.

The colours were de-reddened using the 3D Galactic extinction model of Drimmel et al. (2003). We used the IDL routine provided by the authors of the model to find A_V along the line of sight to the position of the star,² assumed $R_V = 3.1$ (Cardelli et al. 1989) to calculate $E_{B-V} = A_V/R_V$, and adopted the extinction ratios $k = E_X/E_{B-V}$ from Ramírez & Meléndez (2005b) to calculate the colour excess for the other colours.

The uncertainties of E_X are large and difficult to estimate due to A_V , π , R_V and k all having substantial uncertainties. Drimmel et al. (2003) state that ΔA_V due to the model can be as large as $0.2A_V$. We estimated the influence of the parallax uncertainties by calculating A_V at the distance extremes allowed by the parallax uncertainties and found additional relative uncertainty of $\Delta A_V/A_V \approx 20\%$ on average. Finally, while the assumption of a

constant R_V is not well justified, it is unlikely to deviate from the assumed value by more than 10% (McCall 2004). Taking these considerations into account, we assumed $\Delta E_{B-V} = 0.3E_{B-V}$ for all stars. The uncertainties of other colour excesses are slightly larger due to the $\sim 10\%$ uncertainty in the extinction ratios (see, e.g., Taylor 1986).

3.1.2. Surface gravity

The surface gravity $\log g$ (cgs) can be computed from the fundamental relation

$$\log g = \log g_{\odot} + \log \frac{M}{M_{\odot}} + \log \frac{L_{\odot}}{L} + 4 \log \frac{T_{\text{eff}}}{T_{\text{eff},\odot}} \quad (4)$$

by deriving T_{eff} and luminosity L (from photometry and parallax), and then using theoretical stellar evolutionary tracks to get

² <ftp://ftp.to.astro.it/astrometria/extinction/>

Table 2. Spectral lines of interest.

λ , air (nm)	Transition	χ (eV)	log gf (Ref.)	log gf (adopted)
[S I]				
1082.1176	$^3P_2-^1D_2$	0.00	-8.704	-8.704
Fe I				
1081.8277	$^3D_1-^3P_1$	3.96	-1.948	-2.212
1083.3964	$^5D_3-^3F_3$	5.59	-1.019	-1.240
1084.9462	$^5D_4-^5D_3$	5.54	-1.495	-0.650
1086.3519	$^3D_3-^5F_4$	4.73	-0.903	-1.000
1088.1759	$^3P_1-^3F_2$	2.85	-3.553	-3.383
1088.4267	$^3D_2-^3P_2$	3.93	-1.927	-2.075
1089.6300	$^3P_1-^3P_2$	3.07	-2.692	-2.822
Cr I				
1080.1362	$^5D_1-^5D_2$	3.01	-1.715	-1.680
1081.6901	$^5D_2-^5D_2$	3.01	-1.957	-1.920
1082.1658	$^5D_3-^5D_2$	3.01	-1.678	-1.630
1090.5712	$^7P_2-^7S_3$	3.44	-0.647	-0.642

Notes. Wavelengths, excitation energies and oscillator strengths of the lines of interest. The line primarily used for metallicity determination is the Fe I λ 1081.8 nm line. The reference is Froese Fischer & Tachiev (2011) for the sulphur line and the Vienna Atomic Line Database (VALD; Kupka et al. 2000) for the others.

the mass M . Unfortunately, the parallax uncertainties are generally too large to effectively constrain L and M for the stars of this study (see Col. (5) of Table 1). Therefore, we used the PARAM tool³ (da Silva et al. 2006) which adopts two Bayesian priors to take into account the fact that the stars are not distributed randomly on the Hertzsprung-Russell diagram: 1) the masses are distributed according to the lognormal form of Chabrier (2001) initial mass function; 2) the star formation rate has been constant throughout the last 12 Gyr (the maximum age of a star). The theoretical stellar isochrones of Girardi et al. (2000) are then used to compute the probability density functions of M and $\log g$, from which the mean surface gravity and its uncertainty are computed (see da Silva et al. (2006) for a detailed description of the method) and returned to the user. This probabilistic approach allows the derivation of precise surface gravities ($\Delta \log g \sim 0.1$) even when the parallax errors are large ($\Delta \pi / \pi \sim 50\%$). However, we noticed that it breaks down when $\Delta \pi$ approaches and exceeds π , which is the case for 7 stars of our sample.

3.1.3. Metallicity

Since the spectra analysed in this work cover a wavelength range of about 10 nm only, we were forced to derive the metallicity primarily from spectrum synthesis of a single Fe I line at λ 1081.8 nm. However, for about a half of the stars we were able to use secondary metallicity diagnostics (given in Table 2) to verify that the metallicities are not in serious error.

Synthetic spectra were computed with the Spectroscopy Made Easy (SME; Valenti & Piskunov 1996) software using the MARCS model atmospheres of Gustafsson et al. (2008). The main assumptions of the MARCS models are spherical symmetry, hydrostatic equilibrium, flux constancy and local thermodynamic equilibrium. Convection is treated using the mixing-length formalism with mixing-length parameter $\alpha = \ell / H_p = 1.5$ (H_p is the local pressure scale height; Henyey et al. 1965). We

used the α -enhanced models for which $[\alpha/\text{Fe}]$ linearly increases from 0 at solar metallicity and above to +0.4 at $[\text{Fe}/\text{H}] = -1$ and below. The abundances are derived by letting SME do multiple runs, in between which the desired abundances are adjusted, until a satisfactory agreement between synthetic and observed spectra (determined by χ^2 minimization) is achieved. The synthetic spectra are calculated by convolving the theoretical flux spectra with a Gaussian profile to account for macroturbulence and instrumental broadening. The abundances of other α -elements in SME were fixed to be consistent with the MARCS models.

We derived astrophysical $\log gf$ values for the iron lines by fitting these lines in the solar centre intensity spectrum of Wallace et al. (1993) (see Table 2). The resulting $\log gf$ values were tested by producing a synthetic flux spectrum of Arcturus for which the stellar parameters were taken from Ramírez & Allende Prieto (2011). The observations (Hinkle et al. 1995) were well reproduced using the astrophysical $\log gf$ values – for the worst fitting line at 1088.2 nm the $\log gf$ value may be in error by about 0.05 dex, which, when assumed as the uncertainty in the $\log gf$ values, would increase the uncertainties in $[\text{Fe}/\text{H}]$ and $[\text{S}/\text{Fe}]$ by a further ~ 0.02 dex. Astrophysical $\log gf$ values for four chromium lines in the region were also derived because the [S I] line is slightly blended by a Cr I line at λ 1081.7 nm in the coolest/most metal-rich stars of our sample.

We included the molecular species CN (an up-to-date compilation privately provided by B. Plez), C_2 (Querci et al. 1971; U. Jørgensen, private communication) and CH (Jørgensen et al. 1996) in the computations of synthetic spectra.

In our methodology the metallicity is some function of T_{eff} and $\log g$, which itself is some complicated function of T_{eff} . Due to this dependence the uncertainties cannot be added quadratically. But, a conservative estimate of the uncertainties of the metallicities can be obtained by writing the full differential of $[\text{Fe}/\text{H}](T_{\text{eff}}, \log g)$:

$$\Delta[\text{Fe}/\text{H}]_0 = \left| \frac{\partial[\text{Fe}/\text{H}]}{\partial T_{\text{eff}}} \Delta T_{\text{eff}} \right| + \left| \frac{\partial[\text{Fe}/\text{H}]}{\partial \log g} \Delta \log g \right|. \quad (5)$$

Here ΔT_{eff} and $\Delta \log g$ are given by Eq. (3) and PARAM, respectively. An additional uncertainty, mainly due to the uncertainty in continuum placement, is independently introduced by fitting the synthetic profile to the observed profile. This uncertainty was estimated to contribute $\Delta[\text{Fe}/\text{H}]_{\text{syn}} = 0.03$ or 0.06 dex depending on the signal-to-noise ratio of the spectrum. The total uncertainty in metallicity was calculated as

$$\Delta[\text{Fe}/\text{H}] = \sqrt{(\Delta[\text{Fe}/\text{H}]_0)^2 + (\Delta[\text{Fe}/\text{H}]_{\text{syn}})^2}. \quad (6)$$

The two partial derivatives in Eq. (5) were estimated by deriving the change in metallicity due to changes in temperature (gravity) by $\delta T_{\text{eff}} = \pm 50$ K and $\delta T_{\text{eff}} = \pm 100$ K ($\delta \log g = \pm 0.2$ dex and $\delta \log g = \pm 0.4$ dex). This gives four $\delta[\text{Fe}/\text{H}]/\delta T_{\text{eff}}$ ($\delta[\text{Fe}/\text{H}]/\delta \log g$) values, one for each 50 K (0.2 dex) interval, and the mean of these four values was adopted as the approximation to $\partial[\text{Fe}/\text{H}]/\partial T_{\text{eff}}$ ($\partial[\text{Fe}/\text{H}]/\partial \log g$) at the given T_{eff} ($\log g$).

Since $[\text{Fe}/\text{H}]$ has to be known before computing both T_{eff} and $\log g$, it was first adopted from literature (last column of Table 3; see Sect. 4). After the effective temperature and surface gravity were computed, the metallicity of the model atmosphere was adjusted until the best agreement between theoretical and observed spectra was obtained. Since this metallicity was almost always different from the one taken from literature, the stellar

³ http://stev.oapd.inaf.it/cgi-bin/param_1.1

parameters were then recalculated, starting with T_{eff} and ending with $[\text{Fe}/\text{H}]$, until they converged to self-consistent values. One such iteration was typically sufficient to obtain convergence. This procedure lead to an average reduction in the uncertainties of T_{eff} and $\log g$ by about 10%.

3.1.4. Microturbulence

There are too few iron lines to constrain the microturbulence from the spectra. However, since the lines of interest are weak, we were not concerned with precise values of ξ , and were content with estimating them from the $\xi = \xi(T_{\text{eff}}, \log g, [\text{Fe}/\text{H}])$ calibrations privately provided by M. Bergemann (derived for Gaia-ESO), which are accurate to (i.e., the difference from measured values is) about 0.2–0.3 km s^{-1} (standard deviation). A 0.3 km s^{-1} error in ξ introduces a negligible error in the sulphur abundance (0.02–0.03 dex) even for stars with the strongest sulphur lines (e.g., HD 65953).

3.2. Sulphur abundances

The sulphur abundances were derived from the $[\text{S I}]$ line in the same way as the metallicities, once all stellar parameters were determined. The atomic data of the sulphur line were adopted from the compilation of Froese Fischer & Tachiev (2011).

The uncertainties in $[\text{S}/\text{Fe}]$ are

$$\Delta[\text{S}/\text{Fe}] = \sqrt{(\Delta[\text{S}/\text{Fe}]_0)^2 + (\Delta[\text{S}/\text{Fe}]_{\text{syn}})^2}, \quad (7)$$

where $[\text{S}/\text{Fe}]_0$ is the uncertainty due to all stellar parameters (except for ξ) and is given by an expression analogous to Eq. (5) with a third term corresponding to $\Delta[\text{Fe}/\text{H}]$, and we assume that $\Delta[\text{S}/\text{Fe}]_{\text{syn}}$ is also 0.03 or 0.06 dex (because the iron and sulphur lines are of similar strength) but not necessarily the same as $\Delta[\text{Fe}/\text{H}]_{\text{syn}}$. For most stars $\Delta[\text{S}/\text{Fe}]_{\text{syn}}$ is at least equal to $\Delta[\text{Fe}/\text{H}]_{\text{syn}}$ because generally it is more difficult to place the continuum for the sulphur line due to partial blending with the $\text{Cr I } \lambda 1082 \text{ nm}$ line in the red wing and molecular lines in the blue wing.

4. Results

The stellar parameters derived in this work are given in Table 3. For comparison, we also list the literature values, which are the interquartile mean (IQM) values of the entries in the PASTEL catalogue of stellar parameters (Soubiran et al. 2010).⁴

All four stellar parameters have been derived for 29 out of the 39 stars. For the remaining ten stars, all of which have $[\text{Fe}/\text{H}] < -1$, the IQM values of either the surface gravity or the metallicity (or both) were used. For 7 of the 10 stars the parallax errors exceed the measured parallax, and so the surface gravity could not be derived. The metallicity could not be derived for 4 of the 10 stars, because none of the iron lines were detected in their spectra.

Our sample covers effective temperatures from 3900 to 5200 K, surface gravities mainly from 0.5 to 3.0, and metallicities mainly from -2.4 to $+0.2$. In general the formally propagated temperature uncertainties are very small (between 30 and

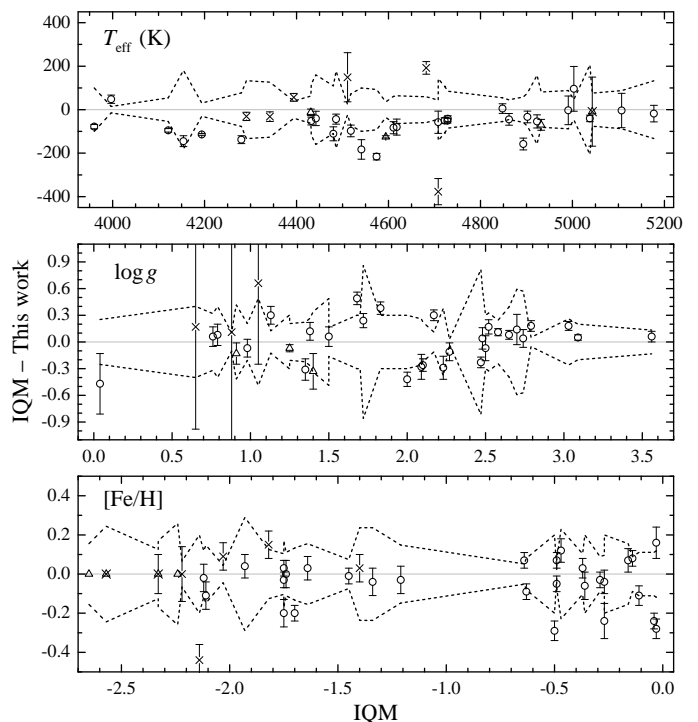


Fig. 1. Differences between stellar parameters from literature (interquartile mean (IQM) values from Soubiran et al. 2010) and the stellar parameters derived in this study versus the literature parameters – top: effective temperatures; middle: surface gravities; bottom: metallicities. The circles correspond to stars with homogeneous stellar parameters, crosses (triangles) denote stars, whose gravities (metallicities) were adopted from literature. The error bars are given by Eq. (3), PARAM (see text) and Eq. (6) for the three respective stellar parameters. The jagged line indicates the uncertainty of literature values ($\text{IQR}/1.35$).

50 K), which indicates that the individual colours give consistent estimates of T_{eff} . Larger uncertainties are associated with fewer colours used or could indicate problems with reddening corrections. The lower limit of 30 K is artificial – for most stars Eq. (3) gives a smaller uncertainty of the effective temperature, which can make the derived surface gravities very sensitive to the exact value of this uncertainty. Therefore, for every star ΔT_{eff} was adjusted to equal the result of Eq. (3) or 30 K, whichever is larger, before calculating its surface gravity, metallicity and sulphur abundance. $\Delta \log g$ are typically 0.1–0.2 dex. Larger values (~ 0.4 dex) are characteristic for the 7 stars with IQM gravities (their uncertainties are calculated as the interquartile range (IQR) divided by 1.35, which would equal 1- σ uncertainties in case of normally distributed values). Uncertainties in $[\text{Fe}/\text{H}]$ are normally below 0.1 dex, but again larger values are typical for the 4 stars with IQM metallicities.

In abundance studies of low-mass main-sequence stars a very tight correlation between the chromium and iron abundances is observed (Bensby et al. 2005), with $[\text{Cr}/\text{H}] \approx [\text{Fe}/\text{H}]$ in stars with $[\text{Fe}/\text{H}] > -1$. Under the reasonable assumption that this correlation extends to giants, we have calculated “updated” metallicities by treating the chromium abundance as another measure of the metallicity.⁵ The updated values are given in Col. (9) of Table 3. As evidenced by the very small changes in the metallicity, the Cr and Fe abundances are indeed nearly equal for the most part. However, to remain consistent throughout the

⁴ Whenever a single value of one of the stellar parameters was referenced multiple times, all but one of duplicate values from different studies by the same first author were discarded to reduce the influence of a single study.

⁵ Logarithm of the number of chromium atoms per 10^{12} hydrogen atoms in the sun: $\log \epsilon(\text{Cr})_{\odot} = 5.64$ (Grevesse et al. 2007).

Table 3. Stellar parameters derived in this and previous works.

HD/BD	This study									Literature data		
	T_{eff}	ΔT_{eff}	$\log g$	$\Delta \log g$	[Fe/H]	$\Delta[\text{Fe}/\text{H}]$	i	ξ	[(Fe+Cr)/H]	T_{eff}	$\log g$	[Fe/H]
2796	5002	30	1.73	0.20	(-2.33)	0.13	...	1.8	...	4932	1.40	-2.33
3546	4977	30	2.44	0.12	-0.54	0.04	1, 2	1.4	-0.64	4923	2.48	-0.63
8724	4790	30	1.66	0.12	-1.55	0.07	1	1.8	...	4574	1.35	-1.75
10380	4216	30	1.48	0.08	-0.23	0.06	1	1.4	-0.20	4121	1.72	-0.27
13979	5052	159	(1.50)	0.49	(-2.57)	0.24	...	1.9	...	5043	1.50	-2.57
21581	5051	30	2.37	0.14	-1.50	0.04	1, 6, 7	1.6	...	4893	2.09	-1.70
23798	4482	33	0.71	0.12	-2.10	0.07	1, 5, 6, 7	2.1	...	4442	0.79	-2.12
26297	4484	30	0.83	0.10	-1.72	0.04	1, 3, 5, 6	2.0	...	4432	1.13	-1.75
29574	4299	30	0.51	0.34	-1.97	0.06	1, 3, 5, 6	2.1	...	4154	0.04	-1.93
34334	4308	30	1.87	0.06	-0.40	0.05	1, 3, 4	1.4	-0.36	4194	2.17	-0.37
36702	4337	30	(0.88)	0.10	-2.12	0.07	1, 3	2.0	...	4394	0.88	-2.03
37160	4771	30	2.57	0.05	-0.59	0.06	1, 3	1.3	-0.56	4729	2.65	-0.47
40460	4724	45	2.42	0.08	-0.21	0.05	1	1.2	-0.29	4541	2.00	-0.50
44007	4907	30	2.36	0.07	-1.67	0.06	1, 3, 6	1.6	...	4862	2.10	-1.64
65953	4038	30	1.19	0.07	-0.30	0.07	1	1.5	-0.28	3960	1.68	-0.36
81192	4779	30	2.46	0.04	-0.71	0.04	1, 2	1.4	-0.74	4728	2.58	-0.64
83212	4616	30	1.26	0.10	-1.44	0.04	1, 5, 6	1.8	...	4518	1.38	-1.45
85773	4443	30	1.00	0.12	(-2.24)	0.24	...	2.0	...	4431	0.91	-2.24
103545	5085	60	(1.70)	0.30	-1.70	0.08	1	1.8	...	4708	1.70	-2.14
110184	4374	30	(0.65)	0.40	-2.33	0.10	1	2.1	...	4342	0.65	-2.33
111721	5078	30	2.56	0.17	-1.30	0.07	1	1.5	...	5038	2.70	-1.34
117876	4772	30	2.35	0.10	-0.44	0.04	1, 2	1.3	-0.41	4722	2.27	-0.49
122563	4719	30	1.32	0.04	(-2.65)	0.16	...	1.9	...	4594	1.25	-2.65
122956	4698	37	1.44	0.11	-1.74	0.07	1	1.8	...	4618	1.50	-1.74
139195	4994	66	2.85	0.05	0.00	0.05	1, 2	1.1	-0.04	4991	3.03	-0.11
161074	3949	30	1.45	0.07	-0.03	0.09	1	1.3	-0.05	3997	1.83	-0.27
166161	5195	38	2.52	0.13	-1.18	0.07	1	1.5	...	5177	2.23	-1.21
168723	4936	30	3.04	0.03	-0.22	0.04	1	1.1	-0.21	4902	3.09	-0.14
184406	4530	30	2.70	0.06	0.20	0.04	1	1.0	0.18	4486	2.47	-0.04
187111	4418	30	0.70	0.11	-1.78	0.04	1, 3	2.1	...	4280	0.76	-1.75
188512	5111	79	3.52	0.06	-0.23	0.06	1, 2	1.2	-0.21	5107	3.56	-0.16
204543	4490	30	(1.25)	0.30	-1.97	0.07	1	1.9	...	4682	1.25	-1.82
212943	4694	30	2.61	0.06	-0.26	0.04	1, 2	1.2	-0.25	4611	2.79	-0.29
214567	4907	103	2.57	0.14	-0.19	0.08	1, 2	1.2	-0.20	5003	2.50	-0.03
216143	4362	113	(1.05)	0.49	-2.22	0.14	1	2.0	...	4511	1.05	-2.22
219615	4843	30	2.39	0.08	-0.56	0.04	1	1.4	-0.53	4848	2.52	-0.49
220954	4766	51	2.70	0.10	0.25	0.05	1	1.0	0.20	4708	2.74	-0.03
221170	4591	32	1.05	0.10	-2.00	0.07	1	2.0	...	4480	0.98	-2.11
+30 2611	4322	30	(0.90)	0.33	-1.43	0.07	1	1.9	-1.41	4291	0.90	-1.40

Notes. The quantities in parentheses denote values that were adopted from literature (i.e., the last two columns). i denotes the Fe I lines used in metallicity determination (ordered according to wavelength as in Table 2). $\Delta\xi$ is about 0.2–0.3 km s⁻¹. Literature data are the interquartile mean values from Soubiran et al. (2010).

metallicity range, the updated metallicities are not considered further.

The stellar parameters derived in this study are plotted against their respective IQM values in Fig. 1. Open circles are used for stars with homogeneous stellar parameters, crosses for stars with IQM surface gravities and triangles for stars with IQM metallicities. The jagged dashed line denotes the uncertainty in the literature values, which is equal to the IQR value divided by 1.35. The error bars are calculated from Eq. (3) in the case of T_{eff} (top panel; notice that some are clearly smaller than the minimum adopted ΔT_{eff} of 30 K), returned by PARAM in case of $\log g$ (middle panel), and calculated from Eq. (6) in case of [Fe/H] (bottom panel).

The sulphur abundances derived in this work are listed in the third column of Table 4 and plotted versus metallicities in Fig. 2. The symbols are the same as in Fig. 1. The start-

ing points of the horizontal (vertical) arrows indicate the upper limits of the metallicities (sulphur abundances). For reference, the abundance of the other α -elements adopted for spectrum synthesis is denoted by the solid line. The lack of stars with $-1.2 < [\text{Fe}/\text{H}] < -0.8$ is a chance outcome. While typical uncertainties of [S/Fe] are 0.1–0.15 dex, $\Delta[\text{S}/\text{Fe}]$ can easily reach ~ 0.4 dex when the stellar parameters are poorly constrained. Some examples of the theoretical spectra (red lines) fitted to observations (black circles) are presented in Figs. 3 and 4, in which a 1 nm wide spectral region containing the forbidden sulphur line is shown. This region also contains the $\lambda 1081.8$ nm iron line used to derive metallicities and two of the four chromium lines listed in Table 2. The positions of these spectral lines are indicated by vertical dashed lines.

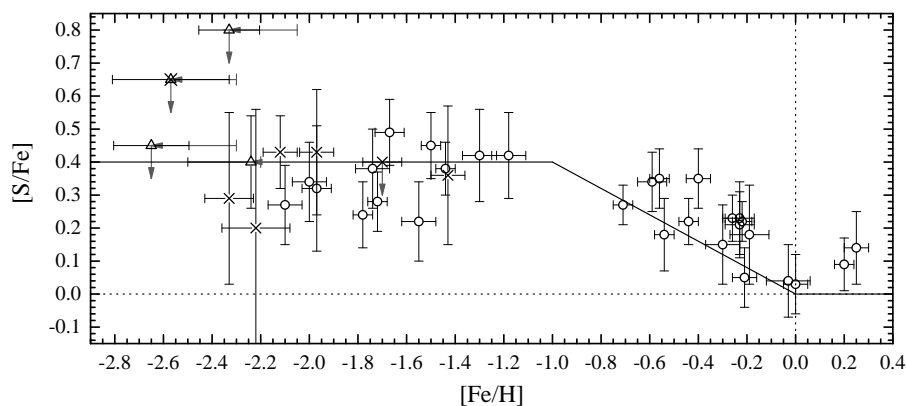


Fig. 2. Sulphur abundances derived in this work. The symbols are the same as in Fig. 1. The starting points of the horizontal (vertical) arrows indicate the upper limit of the metallicity (sulphur abundance). The (upper limit of) sulphur abundance for these stars is derived with respect to the literature (IQM) metallicity. The solid line shows the enrichment assumed for the other α -elements. The dotted lines cross at the solar values, which correspond to $\log \epsilon(\text{Fe})_{\odot} = 7.45$ and $\log \epsilon(\text{S})_{\odot} = 7.14$ (Grevesse et al. 2007).

5. Discussion

In this section we discuss some points concerning our stellar parameters (Sect. 5.1) and sulphur abundances (Sect. 5.2), and then compare our results to previous studies on the Galactic chemical evolution of sulphur (Sect. 5.2.1), and end with comparing our results with theoretical expectations (Sect. 5.2.2).

5.1. Stellar parameters

We find no T_{eff} -dependent differences between the effective temperatures derived from the González Hernández & Bonifacio (2009) calibrations and the interquartile mean effective temperatures. However, the former are systematically hotter by 65 ± 66 K (standard deviation). We also derived the effective temperatures from the calibrations of Ramírez & Meléndez (2005b) and found no statistically significant differences from the IQM temperatures on average. We opted to use the González Hernández & Bonifacio (2009) calibrations for subsequent work anyway because the metallicity binning for each colour used by Ramírez & Meléndez (2005b) results in the calibrated temperatures being discontinuous across the edges of the bins, with a change as small as 0.01 dex in $[\text{Fe}/\text{H}]$ potentially introducing a change of ~ 30 K in T_{eff} for some colours.

The surface gravities and metallicities are found to very closely (to within 0.05 dex) agree on average with the IQM gravities and metallicities.

No non-LTE corrections have been applied to the metallicities derived in this work because we are not aware of any non-LTE calculations of Fe I lines with wavelengths $\lambda > 1000$ nm.

5.2. Sulphur abundances

We plot the sulphur abundances versus metallicities of the whole sample in Fig. 2. Unlike in previous studies by Israelian & Rebolo (2001), Takada-Hidai et al. (2002), Caffau et al. (2005) and Caffau et al. (2010), no stars with extremely high sulphur abundances are observed, nor are the sulphur abundances found to increase towards lower metallicities. In fact, the opposite is observed – a linear fit for the metal-poor ($[\text{Fe}/\text{H}] < -1$) stars with homogeneous stellar parameters gives $[\text{S}/\text{Fe}] = 0.17[\text{Fe}/\text{H}] + 0.63$ – although the significance is low (the standard error of the slope is 0.15) and, when the stars with IQM gravities are included, the trend becomes shallower and insignificant (the slope becomes 0.07 ± 0.12). If the slope is fixed at 0, we get an average abundance of $[\text{S}/\text{Fe}] = 0.35 \pm 0.09$ (standard deviation) for $-2.4 < [\text{Fe}/\text{H}] < -1.1$, which is slightly below the $[\alpha/\text{Fe}] = 0.4$ of the MARCS models. For $-0.8 < [\text{Fe}/\text{H}] < 0.0$ $[\text{S}/\text{Fe}]$ is found

to decrease as the metallicity increases, which is expected of α -elements (solid line). But note that in reality more complicated patterns are observed than assumed in the α -enhanced MARCS models – above $[\text{Fe}/\text{H}] \simeq -0.8$ two distinct trends, corresponding to the Thin and Thick disks, are observed (Bensby et al. 2005; Fuhrmann 2008). According to the models of Kobayashi et al. (2011) the differences for the sulphur trends are, however, less than 0.05 dex.

The uncertainty introduced in the final results ($[\text{S}/\text{Fe}]$) is likely to be large when IQM values of stellar parameters are used. However, the use of IQM values might still be preferred to adopting the values from individual studies unless the missing parameters can be adopted from a single study.

Our formally propagated uncertainties of $[\text{S}/\text{Fe}]$ are comparable to what is usually simply stated in the literature: $\Delta[\text{S}/\text{Fe}] \sim 0.10$ – 0.15 dex. Nevertheless, a detailed breakdown of individual contributions has allowed us to establish that $\log g$ and $[\text{Fe}/\text{H}]$ are the largest contributors to the uncertainty of $[\text{S}/\text{Fe}]$, each introducing a partial error of about 0.05–0.10 dex for most stars. While the forbidden line exhibits low temperature sensitivity (the partial error due to ΔT_{eff} is only about 0.02 dex), our methodology does not take full advantage of this fact, because we use the temperature-sensitive Fe I lines to derive the metallicity. Using lines of singly-ionized iron instead would address this flaw and also reduce the possibility of deviations from LTE affecting the results (Mashonkina et al. 2011; Lind et al. 2012). Unfortunately, no suitable Fe II lines are located in the spectral region around the sulphur line. Overall, we find that the uncertainties in stellar parameters usually dominate the total uncertainty of $[\text{S}/\text{Fe}]$.

Obviously, deriving abundances from a single sulphur line makes each individual of our results more vulnerable to errors, especially at the lowest ($[\text{Fe}/\text{H}] \lesssim -2$) metallicities where the risk of mistaking noise for the iron or sulphur line is increased, and at the highest metallicities because of the possibility of unaccounted weak blends. As stated before, to avoid severe errors in our metallicity estimates, whenever possible we checked whether the metallicities derived from the Fe I $\lambda 1081.8$ nm line are consistent with other, less prominent iron lines in the region.

5.2.1. Comparison with previous studies

In addition to the Ryde (2006) and Jönsson et al. (2011) samples, we have some stars in common with Ryde & Lambert (2004), Takada-Hidai et al. (2005) and Spite et al. (2011), all of who derived the sulphur abundances from the Si I $\lambda 923$ nm lines – Takada-Hidai et al. (2005) used equivalent widths, and Ryde & Lambert (2004) and Spite et al. (2011) performed spectrum

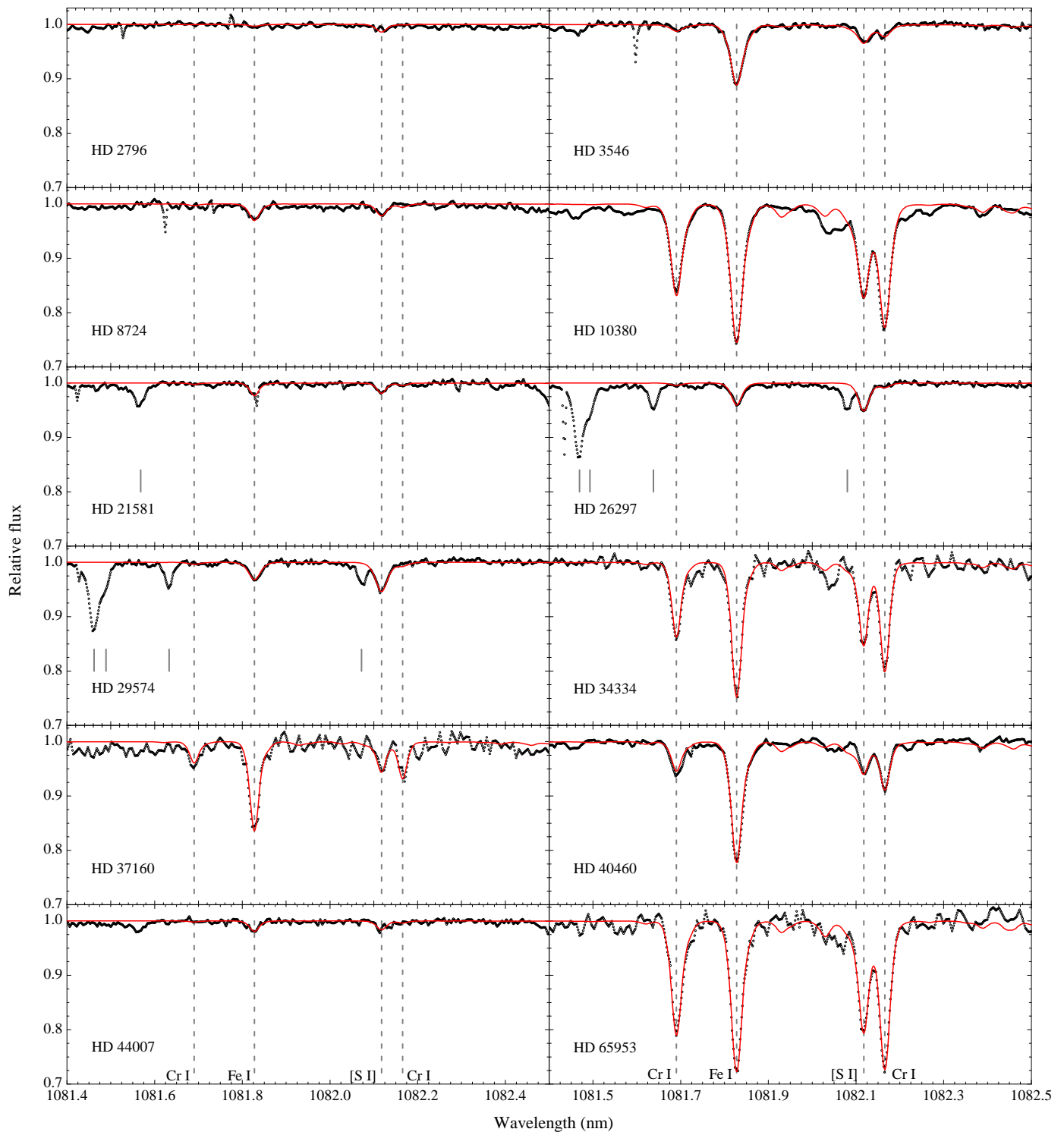


Fig. 3. Synthetic spectra (red line) plotted over the observations (black circles) for a sample of the stars. The positions of important lines are marked by vertical dashed lines. The vertical ticks mark the positions of telluric lines.

synthesis. We list our results along previous results in Table 4. The metallicities and sulphur abundances of previous studies have been translated to the solar chemical composition scale of Grevesse et al. (2007): $\log \epsilon(\text{Fe})_{\odot} = 7.45$ and $\log \epsilon(\text{S})_{\odot} = 7.14$. This scale was adopted to be consistent with the MARCS models. Adoption of the solar abundances from the more recent study of Asplund et al. (2009) would shift all metallicities and sulphur abundances by -0.05 dex and $+0.07$ dex, respectively.

Clearly, there can be major differences in the metallicities and sulphur abundances for individual stars analysed in separate studies. We tested to what extent these differences can be explained by the differences in the stellar parameters. This is particularly important in cases of Ryde (2006) and Jönsson et al. (2011), because these studies analysed the same observational data and used the same spectral diagnostics as this study. And indeed, we find that the differences in $[\text{S}/\text{Fe}]$ can be explained to within ~ 0.05 dex once the differences in stellar parameters are

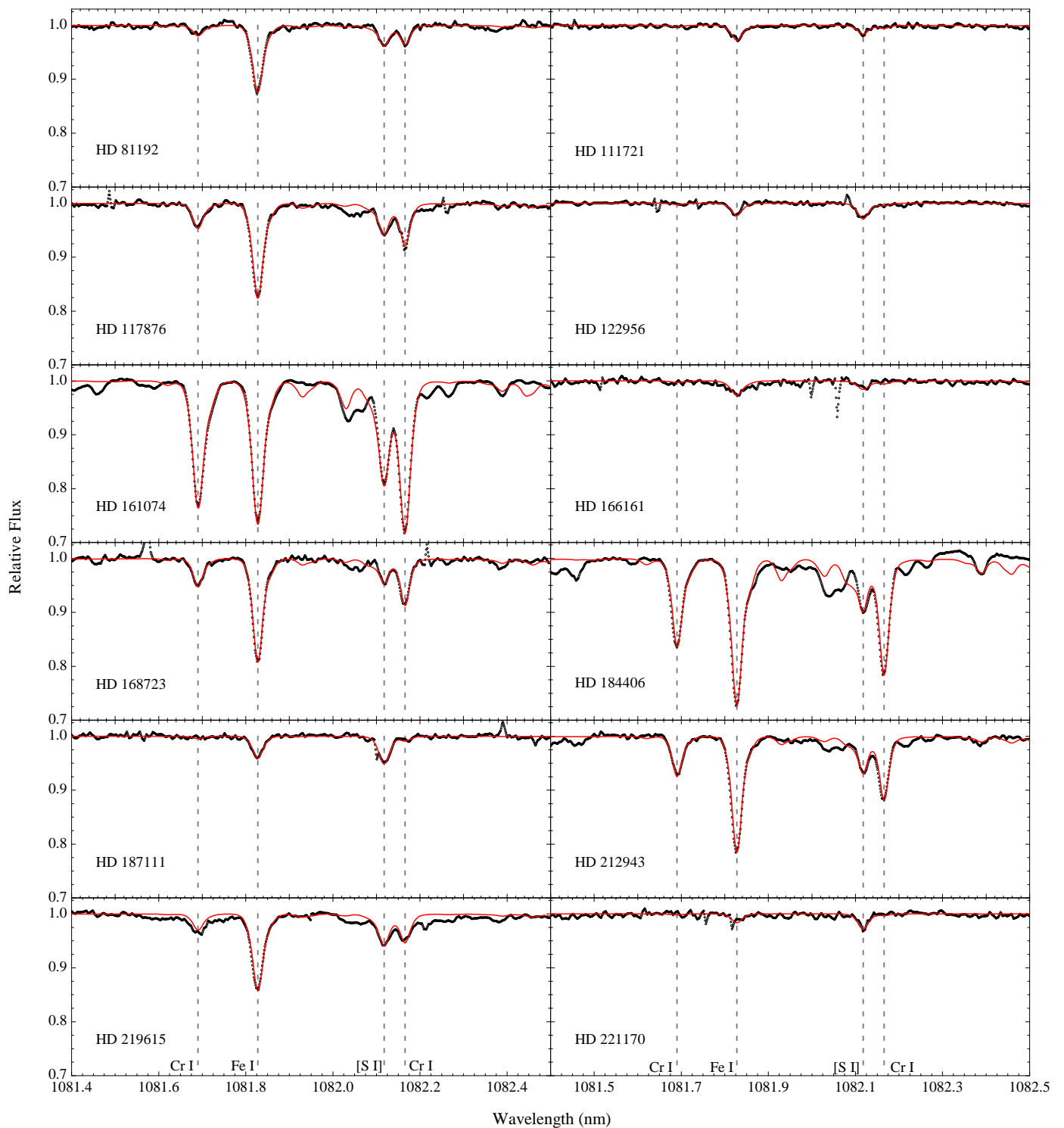


Fig. 4. Synthetic spectra (red line) plotted over the observations (black circles) for a sample of the stars. The positions of important lines are marked by vertical dashed lines.

accounted for. In other words, we can reproduce their results if we adopt the same stellar parameters. The answer to the question of which sulphur abundances are the “correct ones” therefore depends on which stellar parameters one trusts more. Given the significant differences from study to study, the necessity for homogeneous stellar parameters is apparent. Nevertheless, note that systematic differences between stellar parameters from multiple literature sources may not have a noticeable effect on the main conclusions. For example, Jönsson et al. (2011) find a plateau in

[S/Fe] with a scatter (standard deviation) of 0.085 dex. We get virtually the same scatter (0.080 dex) for their stars.

Accounting for the differences in stellar parameters is not always enough when comparing the results to the other studies. For example, consider HD 187111, for which we derive a lower [S/Fe] (by 0.42 dex) than Takada-Hidai et al. (2005) when adopting a higher T_{eff} (by 100 K), lower gravity (by 0.4 dex) and slightly higher metallicity (by 0.07 dex). Differences in stellar parameters account for about a half of the discrepancy in [S/Fe],

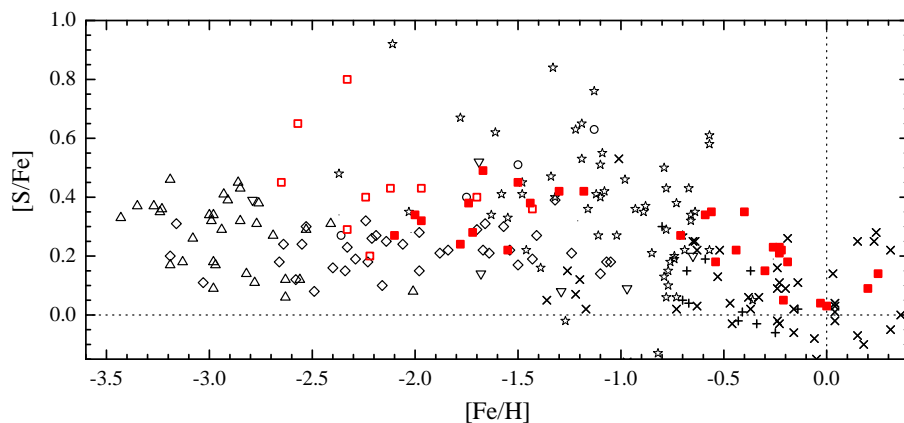


Fig. 5. Sulphur abundances derived in this and previous works. Our results are plotted as red squares (solid for stars with homogeneously determined stellar parameters). The plus symbols are measurements from Chen et al. (2002), crosses are from Takada-Hidai et al. (2002), downwards pointing triangles from Ryde & Lambert (2004), stars from Caffau et al. (2005), rhombi from Nissen et al. (2007), circles from Caffau et al. (2010) and upwards pointing triangles from Spite et al. (2011).

leaving a difference of about 0.2 dex. This remaining difference can be well explained by the strong non-LTE effects of the triplet – the calculations by Takeda et al. (2005) indicate that the result of Takada-Hidai et al. (2005) should be lowered by 0.15 dex. Thus, we argue that HD 187111 has a much lower sulphur abundance than reported in Takada-Hidai et al. (2005).

In some other cases the differences cannot be explained so easily, and remaining differences, which can be around 0.2 dex in $[S/Fe]$, must be due to a combination of a number of factors, for example: 1) quality of observations; 2) accuracy of continuum normalization; 3) completeness and accuracy of atomic and molecular data; 4) uncertainty in the non-LTE corrections; 5) differences in 3D effects; 6) different software used for computing synthetic spectra; 7) different versions of the model atmospheres.

Our mean sulphur abundance below $[Fe/H] = -1$ ($[S/Fe] \approx 0.35$) is significantly ($\sim 2 - 3\sigma$) higher than found in previous studies by Nissen et al. (2007) and Spite et al. (2011), who find mean $[S/Fe] \approx 0.22$ and 0.27 dex, respectively (see Fig. 5). There are three key differences between the studies: 1) the methods used to obtain the stellar parameters in the three studies are different. Nissen et al. (2007) derived T_{eff} from the $H\beta$ line, $\log g$ from Eq. (4) and $[Fe/H]$ from equivalent widths of Fe II lines. Spite et al. (2011) adopted stellar parameters primarily from three different studies, in which T_{eff} was derived from photometric colours and $\log g$ from ionization equilibrium; 2) we use the forbidden line in our analysis, while Nissen et al. (2007) and Spite et al. (2011) use the S I triplet at 923 nm; 3) this sample and that of Spite et al. (2011) consists mainly of giants and subgiants, while the sample of Nissen et al. (2007) mainly comprises dwarf stars. A systematic difference between giants and dwarfs would be a puzzle to solve for model atmospheres. While such a difference may exist, the sulphur abundances derived by Spite et al. (2011) for the few dwarf stars in their sample show good agreement with their results for giants, which argues against this possibility. Systematic differences between the stellar parameter scales and sulphur diagnostics, likely in the form of non-LTE and 3D corrections, are more probable. Calculations by Takeda et al. (2005) and Korotin (2009) have shown that the non-LTE corrections are extremely dependent on temperature and metallicity for metal-poor stars (e.g., the non-LTE corrections for stars with $T_{\text{eff}} = 5000$ and 5500 K at $[Fe/H] = -2$ are $\Delta[S/Fe] \approx -0.4$ and $\Delta[S/Fe] \approx -0.6$ dex, respectively, and at $[Fe/H] = -3$ they are $\Delta[S/Fe] \approx -0.4$ and $\Delta[S/Fe] \approx -0.8$ dex, respectively). It is possible that the non-LTE corrections for the triplet are systematically too large by about 0.1 dex for these types of stars. On a suggestive side note, Jönsson et al. (2011) found their non-LTE-corrected sulphur abundances from the triplet at $\lambda 1045$ nm to be

lower by an average of 0.06 dex (compared to the abundances derived from the forbidden line) in stars of subsample 3. On the other hand, while we emphasize again that the [S I] line forms in LTE, deviations from LTE are still likely important for our sulphur abundances because of their effects on the Fe I lines that were used to derive the metallicities. As stated before, the non-LTE effects of the iron lines with $\lambda > 1000$ nm have not been studied.

Also remember that no attempts have been made to account for 3D effects on the results of this study. Jönsson et al. (2011) used the 3D hydrodynamic model atmospheres of Collet et al. (2007) to estimate that a typical 3D correction for subsample 3 stars might lower the sulphur abundances by about 0.05–0.15 dex, bringing our results in better agreement with previous studies. Negative corrections for the [S I] line are also predicted for metal-poor dwarf stars (Caffau & Ludwig 2007).

Further investigations could test these possibilities from both the observational and theoretical sides. For example, a thorough study analysing the forbidden line, the $\lambda 923$ nm triplet and the $\lambda 1045$ nm triplet in an extended sample of cool metal-poor giants could firmly quantify the systematic differences between the diagnostics, assuming that they are real. Tailored non-LTE calculations using the most up to date model of the sulphur atom and the radiation field from MARCS models would test the differences of the non-LTE aspects of the lines more consistently. More calculations on the line formation of the three diagnostics in 3D stellar atmospheres would allow us to better quantify how reducing the problem to one dimension affects the lines.

Systematic effects concerning the different methods of deriving stellar parameters also deserve a closer inspection. Note that the 65 K difference between our T_{eff} scale and the IQM scale makes the sulphur abundances derived in this work lower by about 0.02 dex when compared to the hypothetical case of no difference.

5.2.2. Comparison with theoretical models

In Fig. 6 we compare our results to the predictions of some of the Galactic chemical evolution models that have been published in literature. In particular, we consider the models by Timmes et al. (1995), Kobayashi et al. (2006), Kobayashi et al. (2011) and Brusadin et al. (2013).

Timmes et al. (1995) consider a simple Galactic chemical evolution model where the Galaxy is formed by a collapse of a massive rotating gas cloud onto an exponential disk and a $1/r^2$ bulge with a gas infall e-folding timescale of 4 Gyr. They assume a Salpeter (1955) initial mass function, a quadratic Schmidt

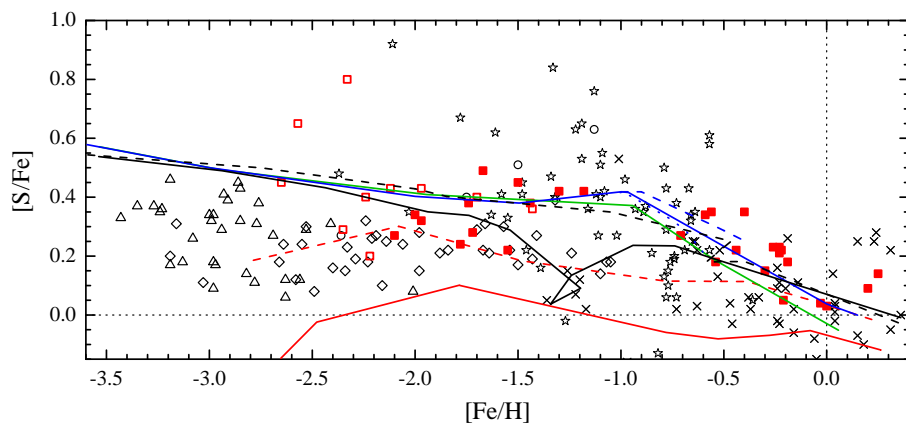


Fig. 6. Comparison to theoretical models of Galactic chemical evolution. The symbols corresponding to previous studies are the same as in Fig. 5. Our results are plotted with solid and empty red squares. The red solid and dashed lines correspond to Timmes et al. (1995) nominal model and one where the iron yields are reduced by a factor of two, respectively. The green line is the prediction of Kobayashi et al. (2006) for the solar neighbourhood. The dotted, solid and dashed blue lines correspond to Halo, solar neighbourhood and Thick disk models of Kobayashi et al. (2011), respectively. The solid and dashed black lines correspond to the Brusadin et al. (2013) double infall model with and without outflow, respectively.

(1963) star formation rate, and instantaneous mixing of yields back into the interstellar medium. They adopt Type II supernovae (SNe) yields from their companion paper (Woosley & Weaver 1995), and yields from low-mass stars and Type Ia SNe from previous works by other authors. According to this model at low metallicities sulphur is produced primarily in explosive oxygen burning in Type II SNe.

Even though some of the assumptions can now be considered outdated, the model manages to reproduce the observed abundance trends for quite a few chemical elements between hydrogen and zinc when, as Timmes et al. (1995) themselves concluded, the iron yields calculated by Woosley & Weaver (1995) are reduced by a factor of 2. Of note is the fact that the model predicts a fairly shallow decline of $[S/Fe]$ starting from $[Fe/H] \sim -2$ (red lines in Figure 6) and a low enrichment of sulphur at all metallicities. The $[S/Fe]$ trend is relatively flat over the metallicity range between $-1 < [Fe/H] < 0$ because the additional sulphur produced in the more metal-rich Type II SNe (from progenitors with total metal content above 10% solar) is balanced by the iron produced in Type Ia SNe.

Kobayashi et al. (2006) simulate the chemical evolution of the solar neighbourhood (using a one-zone model), Galactic Bulge (infall model), Thick disk (infall model) and Halo (closed-box model). They use their own nucleosynthesis yields for Type II supernovae and hypernovae, and the yields from their single-degenerate Type Ia supernovae models. Motivated by observational constraints (the observed $[O/Fe]$ versus $[Fe/H]$), they introduce a “metallicity effect” to delay the onset of SNe Ia in their simulations until $[Fe/H] = -1.1$.

Their simulations predict a slowly changing trend of $[S/Fe]$ below $[Fe/H] \approx -1$, in the solar neighbourhood going from $[S/Fe] \approx 0.5$ at $[Fe/H] \approx -3$ to $[S/Fe] \approx 0.37$ at $[Fe/H] \approx -1$ due to metal-poor and massive SNe producing relatively larger amounts of sulphur. Above $[Fe/H] \approx -1$ an almost linear decrease of $[S/Fe]$ is predicted (green solid line).

Kobayashi et al. (2011) use the same models as Kobayashi et al. (2006) but with some improvements, e.g., they use updated Type II SNe yields, and their chemical evolution model includes yields from stellar winds and asymptotic giant branch stars (Karakas 2010). According to this and the Kobayashi et al. (2006) model at low metallicities sulphur is chiefly produced in Type II SNe with a minor contribution from hypernovae.

Their results predict sulphur trends (blue lines) that are in a very good agreement with their previous results for $[Fe/H] < -1$, while a larger $[S/Fe]$ is predicted at higher metallicities. The predicted differences between the solar neighbourhood (solid line), Thick disk (dashed line) and Galactic Halo (dotted line)

are smaller than observed for other α -elements with the Halo being at most 0.1 dex less enriched in sulphur than the Thick disk at around $[Fe/H] = -0.5$.

Brusadin et al. (2013) adopt the two-infall model originally proposed by Chiappini et al. (1997), to which they add an outflow (wind) from Halo stars. The two-infall model assumes that the Galaxy formed in two primary episodes of primordial gas accretion. During the first accretion episode the Halo and the Bulge are rapidly formed over a timescale of ~ 1 Gyr. In the second episode of much slower accretion the Thin disk is formed “from the inside out”, i.e., the accretion rate decreases with radius (the resulting timescale is ~ 7 Gyr at solar galactocentric radius). The outflow is added to reproduce the observed metallicity distribution function of the Halo. Brusadin et al. (2013) adopt Type II SNe and hypernovae yields from Kobayashi et al. (2006) and Type Ia SNe yields from Iwamoto et al. (1999). In addition they include the yields from asymptotic giant branch stars (Karakas 2010) and novae (Jose & Hernanz 1998).

The main difference between the models with (solid line) and without (dashed line) outflow is the knot at $[Fe/H] \approx -1.3$ predicted by the former, which is caused by a break in star formation not long after the first infall episode. This break coincides with the onset of the first Type Ia SNe (at $[Fe/H] \approx -1.8$) and, as a result, there is a rapid decline in the $[\alpha/Fe]$ - $[Fe/H]$ plane to lower $[\alpha/Fe]$ values. Once the second infall episode starts, the overall metallicity decreases before star formation restarts and $[\alpha/Fe]$ again increases producing the knot.

When stars of all metallicities are considered, the results of this paper are best described by the predictions of the Kobayashi et al. (2011) models, which better describe the results for $[Fe/H] > -1$ than the Kobayashi et al. (2006) and Brusadin et al. (2013) models which predict a similar sulphur enrichment at low metallicities. The Timmes et al. (1995) models are at odds with our results. However, the model with reduced iron yields (red dashed line) fits the results of Nissen et al. (2007) very well. Of the two Brusadin et al. (2013) models, the one with no outflow fits our results slightly better at $[Fe/H] > -1$ and around the knot, but we only have a few stars with this metallicity.

In stars with $-1.5 \leq [Fe/H] \leq -1$ sulphur abundances from $[S/Fe] \sim 0$ to $[S/Fe] \sim 0.8$ have been determined in different studies in the literature. The explanation for finding low enrichment of sulphur might be the sampling of a low- $[\alpha/Fe]$ Halo population, evidence for which has been found both from observations of Halo dwarfs (Nissen & Schuster 2010) and theoretical Λ CDM simulations of the formation and evolution of the Galactic Halo (Zolotov et al. 2010), according to which these low- $[\alpha/Fe]$ stars have formed in satellite galaxies with lower star-

Table 4. The sulphur abundances derived in this and previous works.

HD/BD	This study			Previous studies	
	[Fe/H]	[S/Fe]	Δ [S/Fe]	[Fe/H]	[S/Fe]
8724	-1.55	0.22	0.12
34334	-0.40	0.35	0.09
37160	-0.59	0.34	0.09
65953	-0.30	0.15	0.12
110184	-2.33	0.29	0.26
122956	-1.74	0.38	0.12
166161	-1.18	0.42	0.13
204543	-1.97	0.43	0.19
+302611	-1.43	0.36	0.21
Ryde & Lambert (2004)					
111721	-1.30	0.42	0.14	-1.21	0.32
Takada-Hidai et al. (2005)					
187111	-1.78	0.24	0.10	-1.85	0.66
216143	-2.22	0.20	0.36	-2.15	0.37
221170	-2.00	0.34	0.12	-2.10	0.47
Ryde (2006)					
3546	-0.54	0.18	0.11	-0.60	0.25
10380	-0.23	0.21	0.10	-0.19	0.03
40460	-0.21	0.05	0.09	-0.44	0.00
81192	-0.71	0.27	0.06	-0.56	0.15
117876	-0.44	0.22	0.07	-0.44	0.10
139195	0.00	0.03	0.09	0.02	-0.14
161074	-0.03	0.04	0.11	-0.21	0.20
168723	-0.22	0.22	0.06	-0.13	0.14
184406	0.20	0.09	0.08	0.07	-0.06
188512	-0.23	0.23	0.11	-0.11	0.20
212943	-0.26	0.23	0.07	-0.28	0.21
214567	-0.19	0.18	0.15	0.09	-0.08
219615	-0.56	0.35	0.09	-0.36	0.24
220954	0.25	0.14	0.11	-0.04	0.09
Spite et al. (2011)					
2796	(-2.33)	$\lesssim 0.80$	-	-2.41	0.31
122563	(-2.65)	$\lesssim 0.45$	-	-2.76	0.38
Jönsson et al. (2011)					
13979	(-2.57)	$\lesssim 0.65$	-	-2.26	$\lesssim 0.21$
21581	-1.50	0.45	0.10	-1.64	0.52
23798	-2.10	0.27	0.12	-2.03	0.37
26297	-1.72	0.28	0.09	-1.51	0.41
29574	-1.97	0.32	0.19	-1.70	0.27
36702	-2.12	0.43	0.11	-2.06	0.45
44007	-1.67	0.49	0.10	-1.65	0.37
83212	-1.44	0.38	0.08	-1.40	0.41
85773	(-2.24)	0.40	0.14	-2.36	0.53
103545	-1.70	$\lesssim 0.40$	-	-2.14	$\lesssim 0.52$

Notes. The quantities in parentheses denote values that were adopted from literature (last column of Table 3). The metallicities and abundances of previous studies have been rescaled to correspond to $\log \epsilon(\text{Fe})_{\odot} = 7.45$ and $\log \epsilon(\text{S})_{\odot} = 7.14$ (Grevesse et al. 2007).

formation rates and later accreted by the Milky Way. Distinct Halo populations are not incorporated in the models discussed in this section.

The theoretical [S/Fe] plateaus are slightly higher than we find in this study (except for the models of Timmes et al. 1995) but the agreement with theory is generally better than with the studies of Nissen et al. (2007) and Spite et al. (2011). The important point is that, although detailed quantitative comparison between the models and observations seems premature due to

the relatively large uncertainties in both, our results seem to support the notion that the Galactic chemical evolution of sulphur at low metallicities can largely be explained by production in regular Type II SNe (with, perhaps, some contribution from hypernovae) without the need of invoking additional mechanisms.

6. Conclusions

In this study we have derived the sulphur abundances (or their upper limits) from spectrum synthesis of the [S I] $\lambda 1082.1$ nm line in a sample of 39 stars spanning the stellar parameter ranges $3900 \lesssim T_{\text{eff}} \lesssim 5200$ K, $0.5 \lesssim \log g \lesssim 3.0$ and $-2.4 \lesssim [\text{Fe}/\text{H}] \lesssim 0.2$ by employing one-dimensional local thermodynamic equilibrium MARCS model atmospheres.

The sulphur abundances show almost no dependence on the metallicity for $[\text{Fe}/\text{H}] \lesssim -1$, which is typical for α -elements. This means that the continued rise of [S/Fe] below $[\text{Fe}/\text{H}] \approx -1$ found in some previous studies is not supported by this study, in qualitative agreement with contemporary models of Galactic chemical evolution. However, the uncertainties are large enough that the metallicity range $-1.5 \lesssim [\text{Fe}/\text{H}] \lesssim -1$ should be studied further with a much larger sample of stars.

We manage to derive homogeneous stellar parameters for 29 of the stars (12 with $[\text{Fe}/\text{H}] < -1$) – we use photometric colour-effective temperature calibrations to derive T_{eff} , physical gravities with Bayesian estimation to derive $\log g$, and spectrum synthesis to derive [Fe/H].

Our temperatures, derived from calibrations of González Hernández & Bonifacio (2009), are systematically hotter than the average literature temperatures by about 65 K. At the same time, no systematic effects with respect to literature are found for the surface gravities and metallicities derived here.

The forbidden sulphur line is a valuable diagnostic of sulphur abundances in giant and subgiant stars with $T_{\text{eff}} \lesssim 5200$ K and $[\text{Fe}/\text{H}] \gtrsim -2.3$. The line is insensitive to the assumption of LTE and changes in T_{eff} , but sensitive to changes in surface gravity and metallicity, which makes a homogeneous determination of the stellar parameters necessary. When results across multiple studies are compared, the differences in stellar parameters should be taken into account.

The uncertainties in the stellar parameters are found to dominate the total uncertainties in sulphur abundances. Therefore, the very high S/N values of most of our spectra can be considered a luxury that in future observing campaigns might be sacrificed in favour of observing a larger sample of stars. A S/N > 100 should be enough to derive precise sulphur abundances.

The sulphur abundances derived in this work from the forbidden sulphur line at $\lambda 1082.1$ nm are on average higher than the abundances derived from the triplet at $\lambda 923$ nm in some previous studies (Nissen et al. 2007; Spite et al. 2011). This hints at systematic differences between the stellar parameter scales or the two sulphur diagnostics. In the latter case, we suspect these differences to be due to non-LTE and 3D effects, but further investigation is required.

A worthwhile undertaking would be obtaining a homogeneous set of stellar parameters for the stars in which very high (and low) sulphur abundances have been derived in the past, and re-determining the sulphur abundances in their atmospheres from the forbidden sulphur line when possible.

Acknowledgements. N. R. is a Royal Swedish Academy of Sciences Research Fellow supported by a grant from the Knut and Alice Wallenberg Foundation. Funds from Kungl. Fysiografiska Sällskapet i Lund and support from the Swedish Research Council, VR are acknowledged. The authors are grateful to

L. Lindegren, S. Feltzing and referee E. Caffau for providing valuable feedback that improved the quality of this paper.

References

- Alonso, A., Arribas, S., & Martínez-Roger, C. 1994, *A&AS*, 107, 365
 Alonso, A., Arribas, S., & Martínez-Roger, C. 1998, *A&AS*, 131, 209
 Asplund, M., Grevesse, N., Sauval, A. J., & Scott, P. 2009, *ARA&A*, 47, 481
 Bensby, T., Feltzing, S., Lundström, I., & Ilyin, I. 2005, *A&A*, 433, 185
 Brusadin, G., Matteucci, F., & Romano, D. 2013, *A&A*, 554, A135
 Caffau, E., Bonifacio, P., Faraggiana, R., et al. 2005, *A&A*, 441, 533
 Caffau, E. & Ludwig, H.-G. 2007, *A&A*, 467, L11
 Caffau, E., Sbordone, L., Ludwig, H. G., Bonifacio, P., & Spite, M. 2010, *Astron. Nachr.*, 331, 725
 Cardelli, J., Clayton, G., & Mathis, J. 1989, *ApJ*, 345, 245
 Cayrel, R., Depagne, E., Spite, M., et al. 2004, *A&A*, 416, 1117
 Chabrier, G. 2001, *ApJ*, 554, 1274
 Chen, Y. Q., Nissen, P. E., Zhao, G., & Asplund, M. 2002, *A&A*, 390, 225
 Chiappini, C., Matteucci, F., & Gratton, R. 1997, *ApJ*, 477, 765
 Collet, R., Asplund, M., & Trampedach, R. 2007, *A&A*, 469, 687
 da Silva, L., Girardi, L., Pasquini, L., et al. 2006, *A&A*, 458, 609
 Drimmel, R., Cabrera-Lavers, A., & López-Corredoira, M. 2003, *A&A*, 409, 205
 Francois, P. 1987, *A&A*, 176, 294
 Francois, P. 1988, *A&A*, 195, 226
 Froese Fischer, C. & Tachiev, G. 2011, *MCHF/MCDHF Collection, Version 2*
 Fuhrmann, K. 2008, *MNRAS*, 384, 173
 Girardi, L., Bressan, A., Bertelli, G., & Chiosi, C. 2000, *A&AS*, 141, 371
 González Hernández, J. I. & Bonifacio, P. 2009, *A&A*, 497, 497
 Grevesse, N., Asplund, M., & Sauval, A. J. 2007, *Space Sci. Rev.*, 130, 105
 Gustafsson, B., Edvardsson, B., Eriksson, K., et al. 2008, *A&A*, 486, 951
 Henry, L., Vardya, M. S., & Bodenheimer, P. 1965, *ApJ*, 142, 841
 Hinkle, K., Wallace, L., & Livingston, W. 1995, *PASP*, 107, 1042
 Ilyin, I. V. 2000, PhD thesis, Astronomy Division Department of Physical Sciences P.O.Box 3000 FIN-90014 University of Oulu Finland
 Israelian, G. & Rebolo, R. 2001, *ApJ*, 557, L43
 Iwamoto, K., Brachwitz, F., Nomoto, K., et al. 1999, *ApJS*, 125, 439
 Jørgensen, U. G., Larsson, M., Iwamae, A., & Yu, B. 1996, *A&A*, 315, 204
 Jonsell, K., Edvardsson, B., Gustafsson, B., et al. 2005, *A&A*, 440, 321
 Jönsson, H., Ryde, N., Nissen, P. E., et al. 2011, *A&A*, 530, A144
 Jose, J. & Hernanz, M. 1998, *ApJ*, 494, 680
 Karakas, A. I. 2010, *MNRAS*, 403, 1413
 Kobayashi, C., Karakas, A. I., & Umeda, H. 2011, *MNRAS*, 414, 3231
 Kobayashi, C., Umeda, H., Nomoto, K., Tominaga, N., & Ohkubo, T. 2006, *ApJ*, 653, 1145
 Korn, A. J. & Ryde, N. 2005, *A&A*, 443, 1029
 Korotin, S. A. 2009, *Astron. Rep.*, 53, 651
 Kupka, F. G., Ryabchikova, T. A., Piskunov, N. E., Stempels, H. C., & Weiss, W. W. 2000, *Balt. Astron.*, 9, 590
 Lind, K., Bergemann, M., & Asplund, M. 2012, *MNRAS*, 427, 50
 Mashonkina, L., Gehren, T., Shi, J.-R., Korn, A. J., & Grupp, F. 2011, *A&A*, 528, A87
 McCall, M. L. 2004, *AJ*, 128, 2144
 McWilliam, A. 1997, *ARA&A*, 35, 503
 Mermilliod, J.-C., Mermilliod, M., & Hauck, B. 1997, *A&AS*, 124, 349
 Nakamura, T., Umeda, H., Iwamoto, K., et al. 2001, *ApJ*, 555, 880
 Nissen, P. E., Akerman, C., Asplund, M., et al. 2007, *A&A*, 469, 319
 Nissen, P. E., Chen, Y. Q., Asplund, M., & Pettini, M. 2004, *A&A*, 415, 993
 Nissen, P. E. & Schuster, W. J. 2010, *A&A*, 511, L10
 Querci, F., Querci, M., & Kunde, V. G. 1971, *A&A*, 15, 256
 Ramaty, R., Scully, S. T., Lingenfelter, R. E., & Kozlovsky, B. 2000, *ApJ*, 534, 747
 Ramírez, I. & Allende Prieto, C. 2011, *ApJ*, 743, 135
 Ramírez, I. & Meléndez, J. 2005a, *ApJ*, 626, 446
 Ramírez, I. & Meléndez, J. 2005b, *ApJ*, 626, 465
 Rossi, S., Beers, T. C., Sneden, C., et al. 2005, *AJ*, 130, 2804
 Ryde, N. 2006, *A&A*, 455, L13
 Ryde, N. & Lambert, D. L. 2004, *A&A*, 415, 559
 Salpeter, E. E. 1955, *ApJ*, 121, 161
 Schmidt, M. 1963, *ApJ*, 137, 758
 Skrutskie, M. F., Cutri, R. M., Stiening, R., et al. 2006, *AJ*, 131, 1163
 Soubiran, C., Le Campion, J.-F., Cayrel de Strobel, G., & Caillo, A. 2010, *A&A*, 515, A111
 Spite, M., Caffau, E., Andrievsky, S. M., et al. 2011, *A&A*, 528, A9
 Takada-Hidai, M., Saito, Y.-J., Takeda, Y., et al. 2005, *PASJ*, 57, 347
 Takada-Hidai, M., Takeda, Y., Sato, S., et al. 2002, *ApJ*, 573, 614
 Takeda, Y., Hashimoto, O., Taguchi, H., et al. 2005, *PASJ*, 57, 751
 Taylor, B. J. 1986, *ApJS*, 60, 577
 Timmes, F. X., Woosley, S. E., & Weaver, T. A. 1995, *ApJS*, 98, 617
 Valenti, J. A. & Piskunov, N. 1996, *A&AS*, 118, 595
 van Leeuwen, F. 2007, *A&A*, 474, 653
 Wallace, L., Hinkle, K., & Livingston, W. C. 1993, *An atlas of the photospheric spectrum from 8900 to 13600 cm⁻¹ (7350 to 11230 [angstroms])*
 Wallerstein, G. & Conti, P. 1964, *ApJ*, 140, 858
 Woosley, S. E. & Weaver, T. A. 1995, *ApJS*, 101, 181
 Zolotov, A., Willman, B., Brooks, A. M., et al. 2010, *ApJ*, 721, 738